Summary Report for Contract TAL-NAPC20210119-006

A.C. Kahler
October 2021

Introduction

This report summarizes the work performed under Contract TAL-NAPC20210119-006. The scope of work was determined via a WebEx video conference and subsequent email exchanges between the author and Dr. Jean-Christophe Sublet of the IAEA's Nuclear Data Section. The tasks include (i) a study of the uncertainty associated with Monte Carlo reaction rate and spectral index calculations, with and emphasis on high energy threshold reactions; and (ii) a series of Monte Carlo calculations of the Aspis-Fe88 shielding benchmark. The Aspis-Fe88 calculations utilized existing MCNP input files downloaded from the IAEA's CoNDERC website (https://nds.iaea.org/conderc/aspis) and modified as described in the "Aspis_Fe88 Shielding Benchmark/Experiment" section below.

Reaction Rate and Spectral Index Studies

In order to provide a more complete understanding of the Monte Carlo reaction rate and spectral indices results, a brief review of the basic statistical principals underlying the calculation of means, averages and uncertainties is given. This overview assumes a fundamental knowledge of the subject by the reader and as the formulas noted are well known they are provided without proof or attribution.

The result of any quantity resulting from a Monte Carlo calculation is an average value, $\overline{x}$, and a standard deviation, or uncertainty, σ_x, in that average. If multiple Monte Carlo calculations are undertaken, say N calculations, then there is an alternate method available for computing the uncertainty. Namely to calculate the square root of the sum of the squares of the difference of each individual result minus the N sample average, divided by N-1. Mathematically,

$$\bar{x} = \frac{1}{N}\sum_{i=1}^{N} x_i$$

and

$$\sigma_x = \sqrt{\frac{1}{N-1}\sum_{i=1}^{N}(x_i - \bar{x})^2}$$

When analyzing the output of any complex simulation it is often the case that one or more quantities of interest will be derived from multiple values calculated within that simulation model. An example of this is the calculation of a spectral index, SI. The SI for a specific cross section is the ratio of that cross section's reaction rate divided by (most often) the ^{235}U(n,f) reaction rate. Dividing two Monte Carlo tally values to obtain the SI is trivial but accurately determining the uncertainty of that SI is more complicated.

In particular, the result of dividing two values, $\bar{x}$ and $\bar{y}$, that each have an associated uncertainty is

$$u \pm \sigma_u = \frac{\bar{x} \pm \sigma_x}{\bar{y} \pm \sigma_y}$$

and

$$\sigma_u = u \sqrt{\frac{\sigma_x^2}{\bar{x}^2} + \frac{\sigma_y^2}{\bar{y}^2} - 2\frac{\sigma_{xy}^2}{\bar{x}\bar{y}}}$$

In addition to the $\bar{x}$ and $\bar{y}$ values, and their associated uncertainties there is an additional term, σ_{xy}^2, whose value is often unknown. This term requires knowledge of the individual "x" and "y" values that were used in calculating $\bar{x}$ and $\bar{y}$, and is defined as

$$\sigma_{xy} = \sqrt{\frac{1}{N-1}\sum_{i=1}^{N}(x_i - \bar{x})(y_i - \bar{y})}$$

The impact of the σ_{xy}term on the derived quantity's uncertainty can vary from essentially zero to being an important component to the final value for σ_u. This is illustrated in the following example.

There are three sets of "data" in the Table given below, labelled "Data Set A", "Data Set B" and "Data Set C", respectively, with ten values defined in each set as well as averages and standard deviations for each set. For Data Set A the average and standard deviation are 1.000 ± 0.030. Data Sets B and C contain the same ten values and their average and standard deviation are 0.500 ± 0.015. For this example we will consider Data Set A to represent the ^{235}U(n,f) reaction rate while Data Sets B and C are a reaction rate for which we need to determine the SI. Furthermore, the SI is artificially set to 0.5 by defining the Data Set B values to be 50% of the corresponding Data Set A values. Data Sets A and B are therefore highly correlated, and with each of the ten individual ratios producing the same, 0.500, value the statistical uncertainty on the 10 sample average is zero. For Data Set C we use the same values as in Data Set B but they are listed in a different order, and so there is little correlation between the individual values in Data Sets A and C. Hence the individual SI values, which appear in the "C/A" column, vary from

a low of 0.476 to a high of 0.547 but the ten sample average is once again 0.500, but now with an uncertainty of 0.023.

Table 1: Simulated Data for Correlation Example.					
	Data Set A	Data Set B	Data Set C	B / A	C / A
1	0.955	0.4775	0.5225	0.500	0.547
2	0.965	0.4825	0.4775	0.500	0.495
3	0.975	0.4875	0.5175	0.500	0.531
4	0.985	0.4925	0.4825	0.500	0.490
5	0.995	0.4975	0.5125	0.500	0.515
6	1.005	0.5025	0.4875	0.500	0.485
7	1.015	0.5075	0.5075	0.500	0.500
8	1.025	0.5125	0.4925	0.500	0.480
9	1.035	0.5175	0.5025	0.500	0.486
10	1.045	0.5225	0.4975	0.500	0.476
Average	**1.000**	**0.500**	**0.500**	**0.500**	**0.500**
Stdev.s (pop)	**0.030**	**0.015**	**0.015**	**0.000**	**0.023**
		B / A	C / A		
"SI"		0.500	0.500		
"SI" σ (σ_A & σ_B (or σ_C) only)		0.021	0.021		
"SI" σ (using all uncertainty components)		**0.000**	**0.023**		

If we have only run a single Monte Carlo calculation what the code gives us is simply the average and its standard deviation. Those values, highlighted in bold and noted previously, are 1.000 ± 0.030, 0.500 ± 0.015 and 0.500 ± 0.015 for Data Sets A, B and C, respectively. With only this information in hand the SI for either ratio is 0.500 and the uncertainty in the ratio is simply the root-mean-square of the individual variances. Hence, we report a spectral index of 0.500 ± 0.021 for both B/A and C/A.

However, suppose we had run ten independent Monte Carlo calculations, and so we now know the ten individual values that define Data Set's A, B and C averages. It is now possible to calculate ten individual SIs, which are tabulated in the Columns labelled "B / A" and "C / A" and use that additional knowledge to calculate a more accurate standard deviation. There are two ways to calculate these uncertainties. One is to use the ten individual SI values from the "B / A" or "C / A" columns, yielding 0.500 ± 0.000 or 0.500 ± 0.023 respectively. Alternatively, the equation provided previously for σ_u can be used. Either method will yield a 0.023 uncertainty.

Clearly this is an artificial example meant to highlight how the $\sigma_u$value can be influenced by the σ_{xy} term. An important observation whose significance will become clear shortly is to notice when the two data sets that comprise the SI vary in a similar manner, i.e., are correlated, then

the SI uncertainty is significantly less than that predicted by calculating the square root of the sum of the individual data set variances. In the above example 0.000 versus 0.021. Or, if there is little relationship in how the individual values in the respective data sets vary (i.e., are uncorrelated) then the SI uncertainty is more likely to be accurately reflected by this square root sum, e.g., 0.021 versus 0.023 in the above example. An immediate follow-up question is "How does this relate to the most common occurrence of users running a single Monte Carlo calculation for their system of interest?".

For example, consider the Godiva critical assembly. This is a nearly spherical, minimally reflected, assembly consisting of nested hemispherical shells of highly-enriched uranium (HEU). The computer model is a bare HEU sphere in vacuum. Reaction rate measurements are made by irradiating foils or small fission counters positioned at or near the core center. And reaction rate calculations are performed by specifying the appropriate tally definitions over a small volume located in the center of the sphere.

For a given tally definition we simply obtain a reaction rate and its uncertainty. Internal to the code however are a multitude of calculations to estimate the energy-dependent flux in the region of interest and when multiplied by the cross section provide an estimate of the reaction rate for that particular collision. When the simulation concludes the reported reaction rate, and its uncertainty, are reported to the User. And so, the calculated reaction rate is essentially an approximation of the integral over space and energy of the flux multiplied by the cross section.

A number of MCNP jobs have been run for the Godiva critical assembly and in the following Table we provide the calculated reaction rates and uncertainties for three cross sections, ^{235}U(n,f), ^{239}Pu(n,f) and ^{90}Zr(n,2n), plus the calculated SIs, under two conditions. The first set of reaction rates are those obtained from a single, one billion history, MCNP job. The resulting uncertainties for the ^{235}U(n,f) and ^{239}Pu(n,f) reaction rates are approximately 0.09%. The ^{90}Zr(n,2n) reaction rate is less well determined as its uncertainty is estimated at 9.4%. The resulting SIs are now calculated; 1.3845±0.0018 for ^{239}Pu(n,f) and 4.9e-5±0.5e-5 for ^{90}Zr(n,2n). This is a typical result; namely a single Monte Carlo job is executed for a User determined number of histories that is expected to provide sufficient precision for that application.

Table 2. Selected Reaction Rates and Spectral Indices			
Cross Section	Reaction Rate	Uncertainty	Comment
^{235}U(n,f)	6.33120e-3	0.09%	Results are from a single, one billion neutron history simulation.
^{239}Pu(n,f)	8.76523e-3	0.09%	
^{90}Zr(n,2n)	3.12262e-7	9.4%	
Spectral Index	SI Value	SI Uncertainty	Comment
^{239}Pu(n,f) / ^{235}U(n,f)	1.3845	0.0018	SI uncertainty is based upon individual uncertainties alone.
^{90}Zr(n,2n) / ^{235}U(n,f)	0.000049	0.000005	

Cross Section	Reaction Rate	Uncertainty	Comment
^{235}U(n,f)	6.33003e-3	0.10%	Results are from 100, one billion neutron history simulations.
^{239}Pu(n,f)	8.76374e-3	0.10%	
^{90}Zr(n,2n)	3.45319e-7	10.6%	
Spectral Index	SI Value	SI Uncertainty	Comment
^{239}Pu(n,f) / ^{235}U(n,f)	1.3845	0.0002	Uncertainty includes correlation.
^{90}Zr(n,2n) / ^{235}U(n,f)	0.000055	0.000006	

As a numerical exercise the MCNP simulation had been repeated 100 times; each job comprising one billion neutron histories and each job utilizing a different random number sequence so that each of the 100 results are independent of one another. Continuing down the Table we again tabulate the individual reaction rates, with the 100-sample average values being 6.33003e-3 for ^{235}U(n,f); 8.76374e-3 for ^{239}Pu(n,f) and 3.45319e-7 for ^{90}Zr(n,2n). The uncertainties, 0.10%, 0.10% and 10.6%, respectively are for the 100-sample population. As expected, these reaction rate values and their uncertainties are similar to the results in the top half of the Table. The resulting SIs are also similar with 1.3845 obtained for ^{239}Pu(n,f) and 5.5e-5 obtained for ^{90}Zr(n,2n). The same cannot be said for the ^{239}Pu(n,f) uncertainty which at 0.0002 is an order of magnitude smaller than the 0.0018 uncertainty from the single job example. In contrast, for ^{90}Zr(n,2n) the SI uncertainty is approximately 10% (4.9e-5±5.0e-6 or 5.5e-5±6.0e-6) in either case.

Knowledge of the underlying cross sections can qualitatively explain this difference. Illustrated below is the calculated flux in the central region of the Godiva assembly, as well as NJOY processed cross sections for the ^{235}U(n,f), ^{239}Pu(n,f) and ^{90}Zr(n,2n) reactions. The cross sections are displayed in multi-group form for the UK 1102-group energy structure.

Recall that the reaction rate is calculated as a product of the flux times the cross section. For Godiva the flux extends over a broad energy range, peaking in the several hundred keV to a few MeV energy range. The ^{235}U(n,f) and ^{239}Pu(n,f) cross sections are continuous over this range and exhibit a similar structure. As such there is a high degree of correlation in these cross sections and their respective reaction rates will fluctuate in tandem with variations in the calculated flux. And just as was observed in the artificial example with highly correlated Data Sets A and B, the resulting statistical uncertainty on the ratio is significantly less than that obtained by a simple square root of the sum of individual variances. In contrast, the (n,2n) cross section in the ^{90}Zr evaluation, which only extends to 20 MeV, has a threshold in excess of 10 MeV. The shape and average energy in this flux spectrum of this threshold reaction cross section bears no resemblance to the ^{235}U(n,f) cross section and so there is no expectation that the ^{90}Zr(n,2n) and ^{235}U(n,f) reaction rates will fluctuate in a similar fashion to variations in the

flux. In the context of the artificial example these reaction rates are uncorrelated just as the values in Data Sets A and C were uncorrelated. Hence the calculated uncertainty from a single job is an accurate representation of this SI's uncertainty.

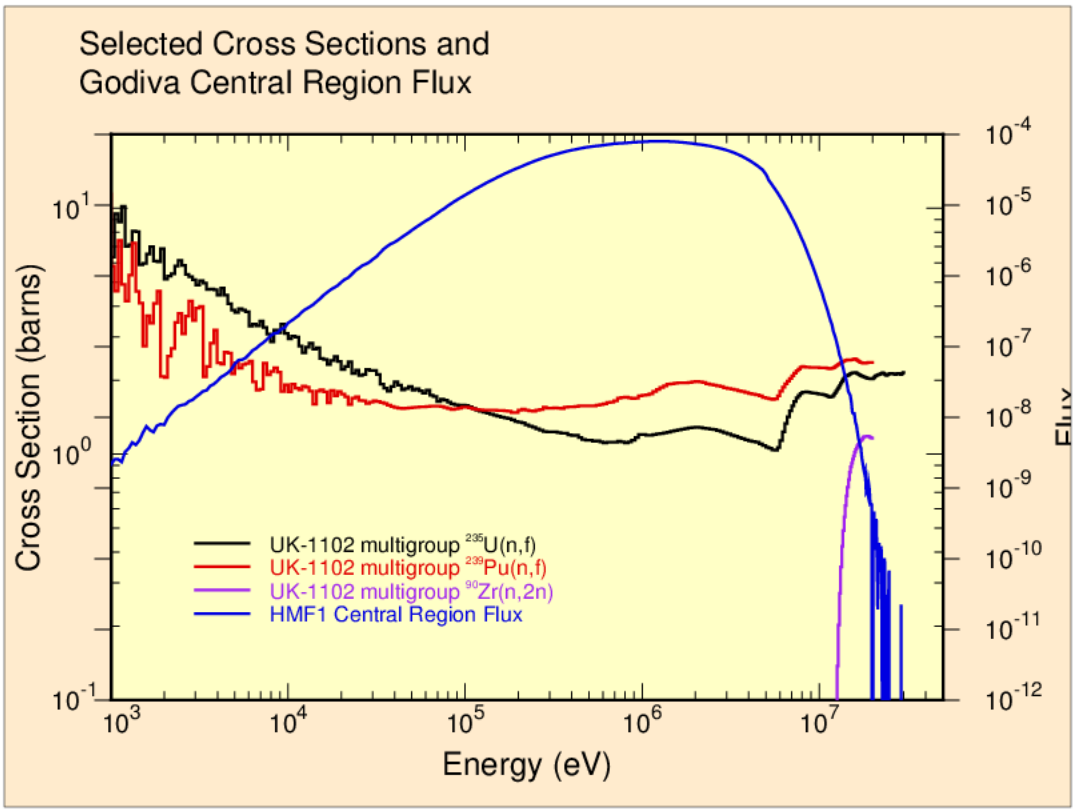

Unfortunately, this study does not, and cannot, produce a quantitative method to account for the effect of correlation in the SI uncertainty. Rather we simply point out that knowledge of the underlying cross sections and a qualitative understanding of their similarity or lack thereof can provide an indication to the User as to the accuracy of the SI uncertainty.

Prior to closing this Section, we make one further observation. This author's experience has been that one rarely knows when first running a simulation with reaction rate definitions the total suite of reactions that will be of interest. This then leads to the need to rerun the simulation with the additional reaction tallies, perhaps multiple times. However, if the initial simulation includes a detailed energy-dependent flux tally then any reaction rate may be calculated offline. For example, the following Table lists reaction rate tallies for ^{235}U(n,f), ^{239}Pu(n,f) and ^{90}Zr(n,2n) from a single 100 billion history MCNP job of the Godiva critical assembly. This job also included an energy-dependent flux tally using the UK 1102-group energy structure. With NJOY one can calculate the ^{235}U(n,f), ^{239}Pu(n,f) and ^{90}Zr(n,2n) multigroup cross sections for this same energy structure. Placing the multigroup flux and multigroup cross sections in a spreadsheet and utilizing the "sumproduct" function

approximates the Monte Carlo reaction rate calculation. The results of these calculations are shown in the "NJOY" Reaction Rate column.

Table 3. MCNP and Offline Reaction Rates			
Cross Section	MCNP Reaction Rate	"NJOY" Reaction Rate	NJOY / MCNP
^{235}U(n,f)	6.32858e-3	6.32949e-3	1.0001
^{239}Pu(n,f)	8.76161e-3	8.76171e-3	1.0000
^{90}Zr(n,2n)	3.46815e-7	3.44351e-7	0.9929

The offline ("NJOY") reaction rate calculations for ^{235}U(n,f) and ^{239}Pu(n,f) are in excellent agreement with MCNP. The agreement is also relatively good for ^{90}Zr(n,2n); although the coarse energy structure in the 10 to 20 MeV energy range has an impact.

The Aspis_Fe88 Shielding Benchmark/Experiment

Information on the Aspis_Fe88 is shielding benchmark is available in the SINBAD Shielding Handbook. Included in SINBAD's Aspis section is AEA Report AEA-RS-1231, "Benchmark Testing of JEF2.2 Data for Shielding Applications: Analysis of the Winfrith Iron 88 Benchmark Experiment", by G.A.Wright and M.J.Brimstone. The summary description of the measurement and facility provided in the next several paragraphs is taken from this document.

"… The ASPIS shielding facility is installed on the NESTOR reactor at Winfrith. NESTOR is a light water cooled, graphite and light water moderated reactor which operates at powers of up to 30 kW and is used as a source of neutrons for a wide range of applications. The core of the reactor, which comprises 26 MTR (Materials Test Reactor) type fuel elements, is contained within an annulus formed by two concentric aluminum vessels through which water circulates. The inner vessel is tilled with graphite to form an inner reflector. The outer tank is surrounded by an external graphite reflector in the form of a block having dimensions 182 cm x 182 cm x 122 cm which contains the control plate slots adjacent to the vessel wall. Leading off each of the four faces of the external reflector is an experiment cave which can be isolated from the reactor by shutters composed of boral or combinations of neutron/gamma-ray shield materials.

ASPIS is located in the NESTOR cave C. Shield components, which are in the main slabs or tanks, are mounted vertically in a mobile tank which has an internal cross-sectional area of 1.8 m x 1.9 m and a length of 3.7 m. A fission plate is located within the experimental shield array. The loaded tank is moved into the cave where thermal neutrons leaking from the outer graphite reflector of NESTOR are used to drive the fission plate to provide a well defined neutron source for penetration measurements. The fission plate is manufactured from 93% enriched uranium/aluminium alloy and approximates to a disc source with an effective radius of 56 cm and a thickness of 2 mm. The absolute source strength is determined by fission product

counting and the spatial distribution via detailed low energy flux mapping with activation detectors.

The [Iron 88 Benchmark experimental] array comprises three regions; the source region containing moderator and the fission plate, the shield made from 13 mild steel plates, each of approximately 5.1 cm thickness, and a deep backing shield manufactured from mild and stainless steel. To allow detector access within the shield 6 mm spacers are placed between each slab component. In practice the depth of the air gaps varies owing to positional uncertainties of the plates and their flatness. The 6 mm gap is therefore nominal and an average gap of 7.4 mm was measured for the experiment. …"

Measurements were made for a variety of Monitor reactions at various locations in the shield. The Monitor reactions include $^{27}Al(n,\alpha)^{24}Na$, $^{32}S(n,p)^{32}P$, $^{103}Rh(n,n')^{103m}Rh$, $^{115}In(n,n')^{115m}In$, and Cd covered $^{197}Au(n,\gamma)^{198}Au$. The respective cross sections at keV energies and above are shown in the following Figure. As is readily apparent the various cross sections probe higher and higher energies in neutron transport through these shields.

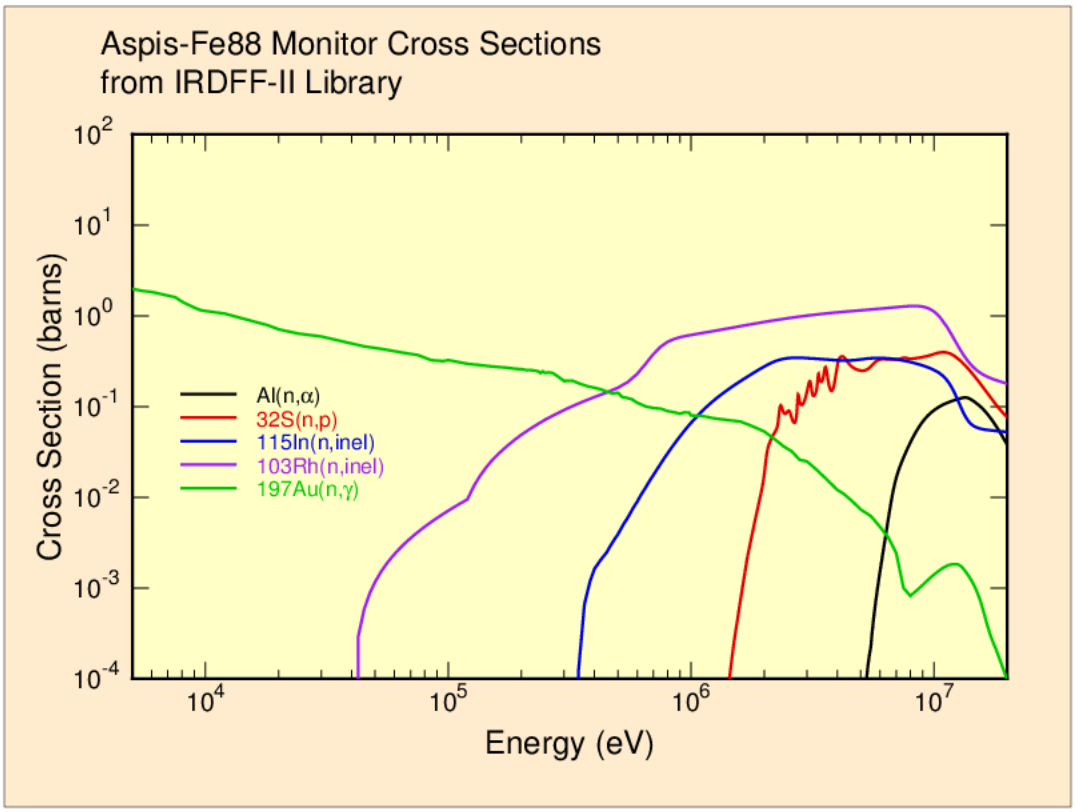

The following Figures contain the results of legacy and new calculations for this benchmark. In all cases the Figure layout is the same; namely (i) red "x" symbols (without error bars) show previously obtained C/E values for the respective Monitor reactions using ENDF/B-VIII.0

transport and IRDFF-v1.05 Monitor nuclear data; (ii) black squares with error bars provide C/E values for calculations using ENDF/B-VIII.0 ACE transport and IRDFF-II dosimetry nuclear data that were performed during this contract and (iii) orange circles with error bars provide C/E values when the ENDF/B-VIII.0 ^{54,56}Fe transport nuclear data were exchanged for preliminary TENDL-2021 ^{54,56}Fe transport nuclear data.

The previous, or "legacy" calculations, are available on the CoNDERC website (https://nds.iaea.org/conderc/aspis). They, and the black square calculations both use ENDF/B-VIII.0 transport cross sections but the legacy Monitor nuclear data come from IRDFF-v1.05 whereas the new calculations utilized IRDFF-II. For these Monitors only the ^{197}Au(n,γ) cross sections differ between IRDFF-v1.05 and IRDFF-II. Also, all but the Au monitor calculations utilized existing wwinp files, and were run for 10x the number of neutron histories as were run previously. The new Au Monitor calculations lack a wwinp file and were run for the same number of neutron histories as the previous calculation.

In one case a small input error was discovered. In the ^{115}In Monitor's MCNP input file the number density assigned to ^{115}In at the A7 location was incorrect. The correct value is 0.0362878 but ^{32}S's value of 0.0361182 was inadvertently used. Fortunately, this is a small error, as the incorrect data are only wrong by about 0.5% and is masked by the stochastic uncertainty in the Monte Carlo calculation which is of a similar magnitude.

Brief comments follow for the various Monitor C/E results.

For $^{32}S(n,p)^{32}P$ monitor calculations there is little change in calculated C/E between the previous (IRDFF-v1.05) and new (IRDFF-II) calculations. At the nearest, A2, measurement position there is about a 10% bias (low) in C/E and this negative bias increases with deeper penetration into the shield, reaching nearly 40% at the deepest penetration, A15, measurement location. Replacing ENDF/B-VIII.0 $^{54,56}Fe$ data with preliminary TENDL-2021 $^{54,56}Fe$ cross sections produces a significant improvement. The initial 10% bias remains but is now approximately constant at all measurement locations.

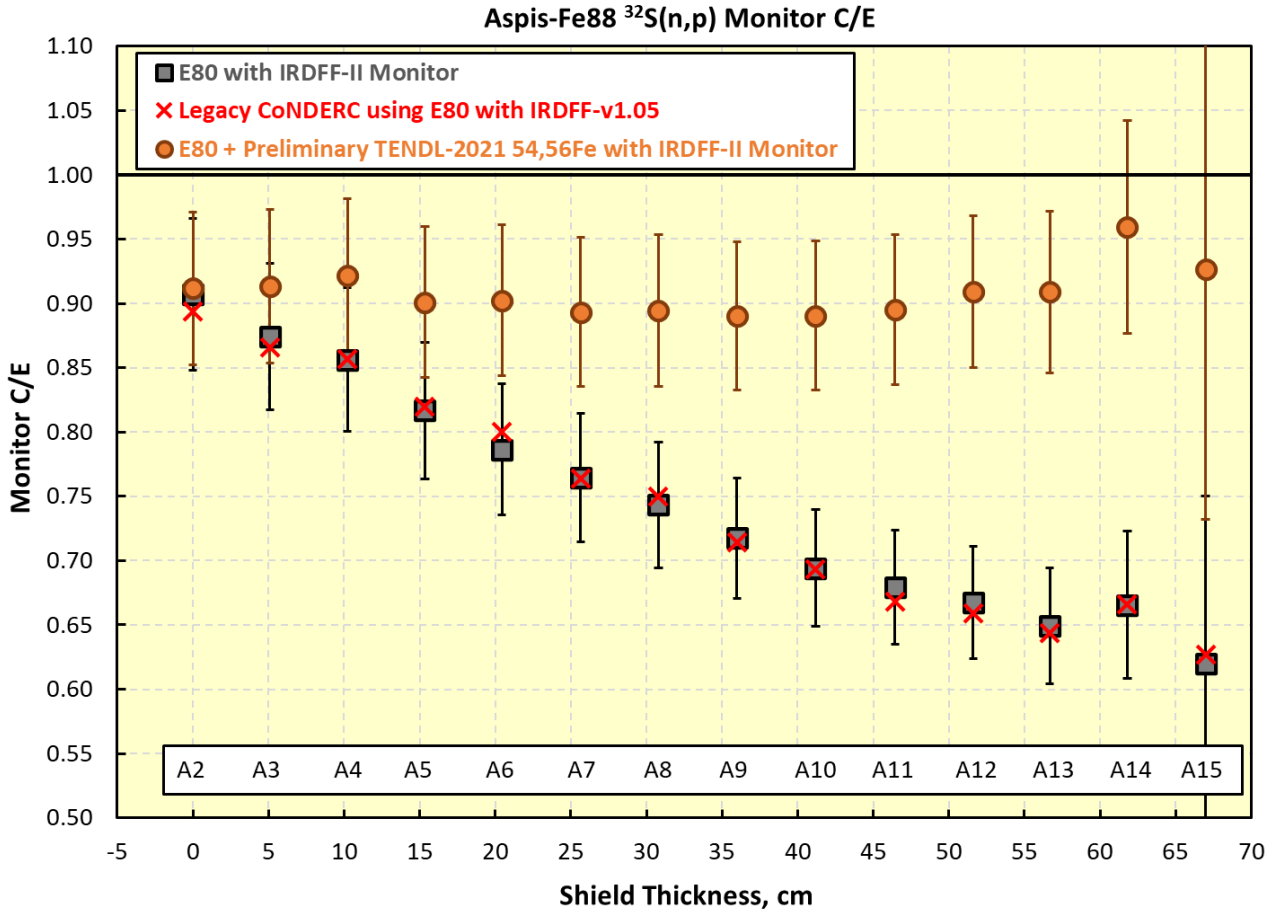

For ^{103}Rh(n,n')^{103m}Rh, all calculations exhibit a similar C/E behavior. Namely a small, approximately +5% bias at the initial measurement position followed by a consistent decrease in C/E at increasing depths through the shield. The final bias is in the -5% to -10% range. The combined measurement plus calculated uncertainty is of a similar magnitude to this bias, but the trend over many measurement points suggests the observed variation with shield penetration is real.

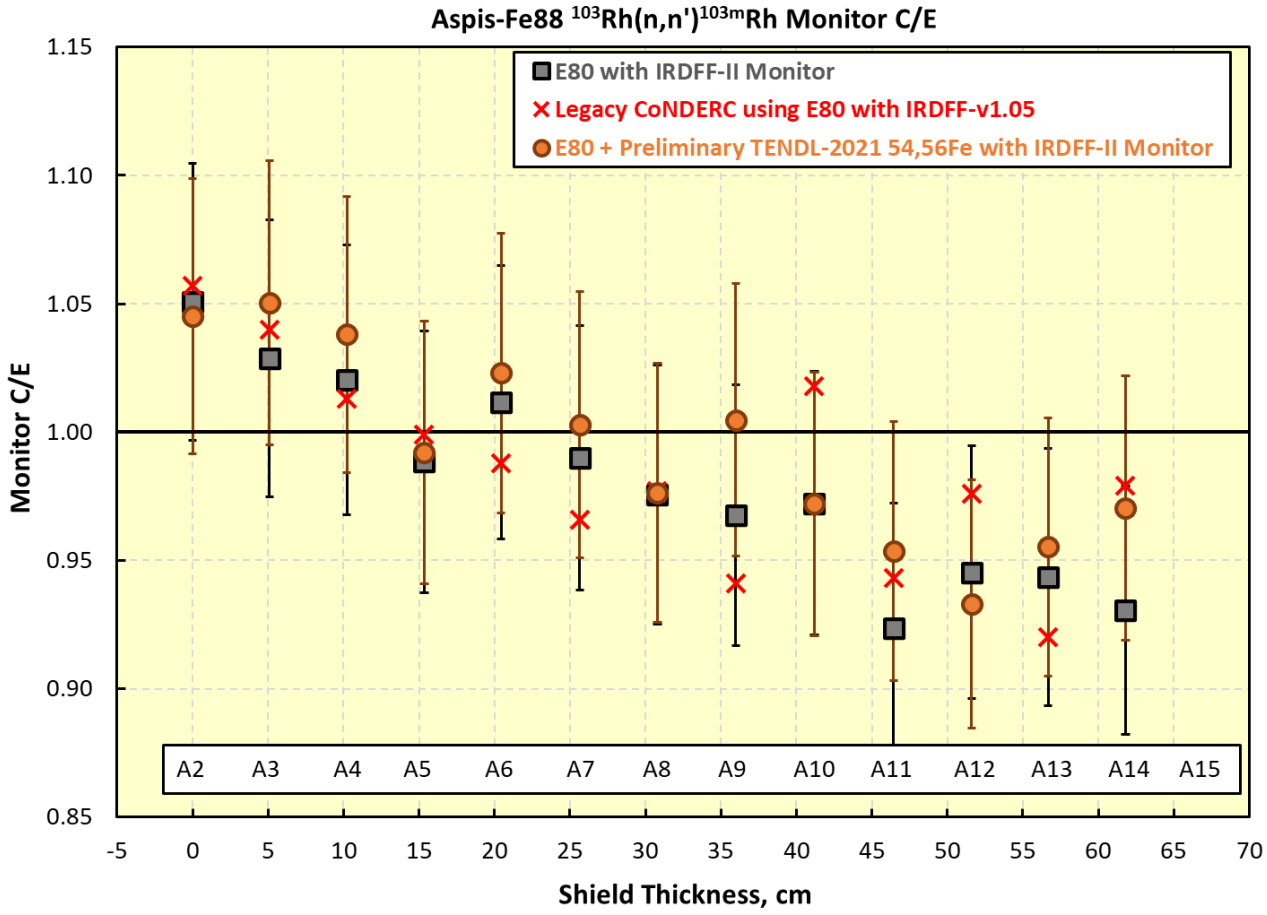

The ^{115}In(n,n')^{115m}In C/E values follow a similar pattern as those from the ^{103}Rh monitor, but here the initial C/E value is essentially unity and the decreasing C/E trend with shield depth is more pronounced. At the deepest penetration the bias is approximately -20%.

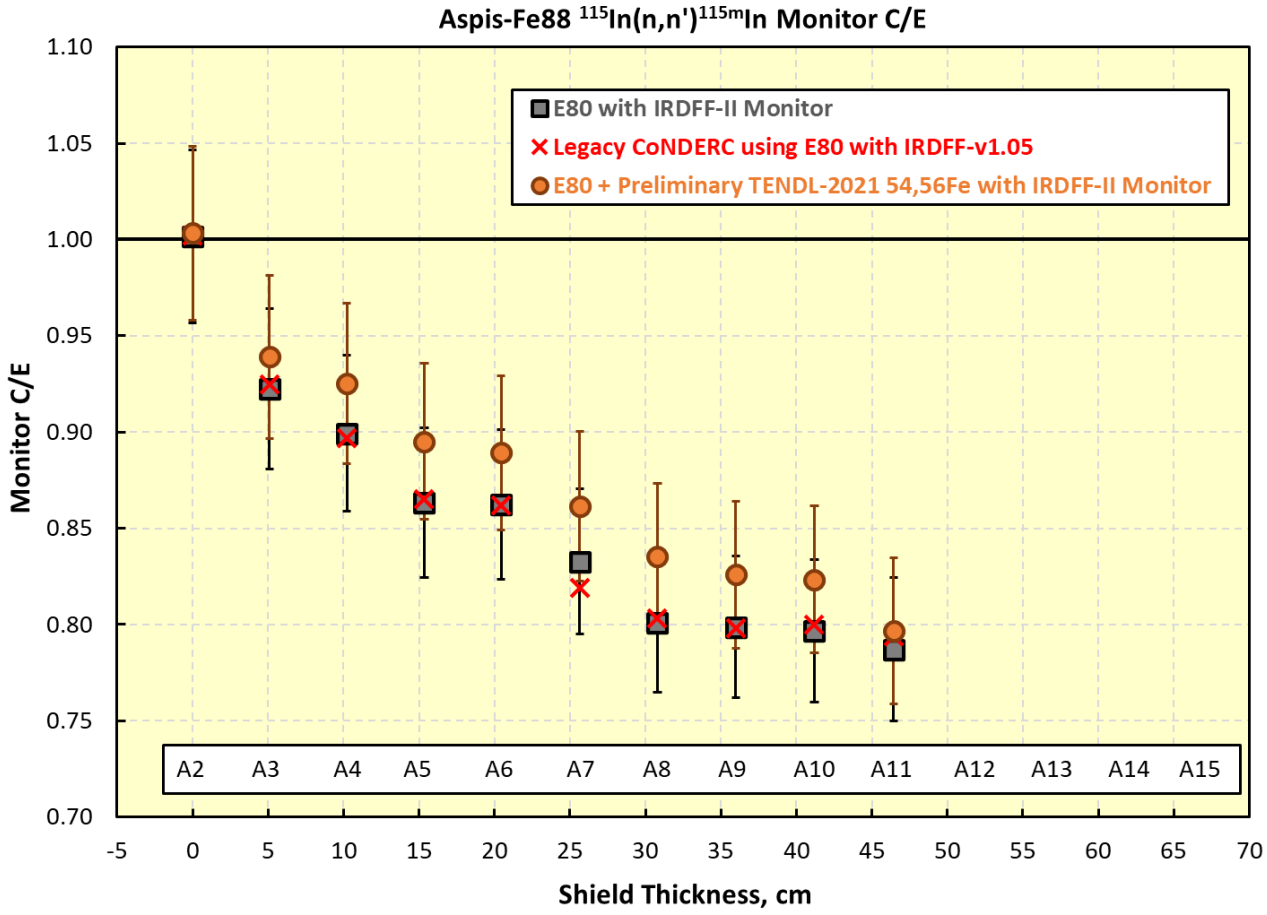

The Cd-covered $^{197}Au(n,\gamma)^{198}Au$ ENDF/B-VIII.0 C/E values are generally close to unity for measurement positions A2 thorough A10 followed by a -5% to -15% bias in A11 to A15 locations. C/E values with the preliminary TENDL-2021 $^{54,56}Fe$ cross sections are typically 5% to 10% or so larger, exhibiting a small positive bias in the A2 to A10 positions before dropping to near unity for the A11 to A15 locations.

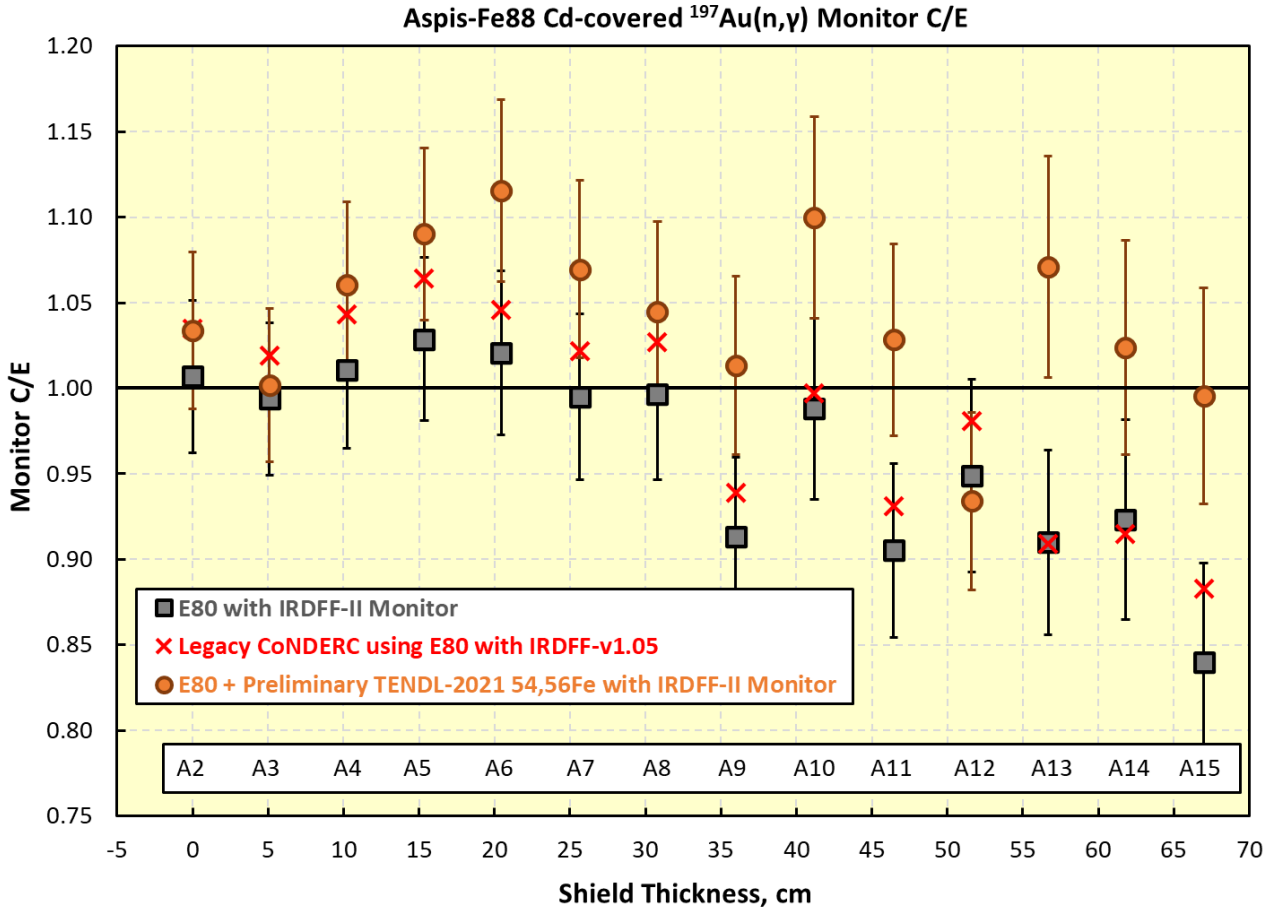

C/E values for the ^{27}Al(n,α) measurement are poor. Legacy and new ENDF/B-VIII.0 calculations produce C/E values that are approximately 10% to 15% high. When the preliminary TENDL-2021 ^{54,56}Fe cross sections are used the bias is significantly worse, exhibiting a linear trend with shield depth of +35% to +70%.

The ^{27}Al(n,α) reaction threshold is significantly higher than the reaction threshold for the other Monitor reactions. The maximum cross section occurs near 13 MeV and so these results suggest the preliminary ^{54,56}Fe cross sections in the 10 MeV to 15 MeV range may be deficient.

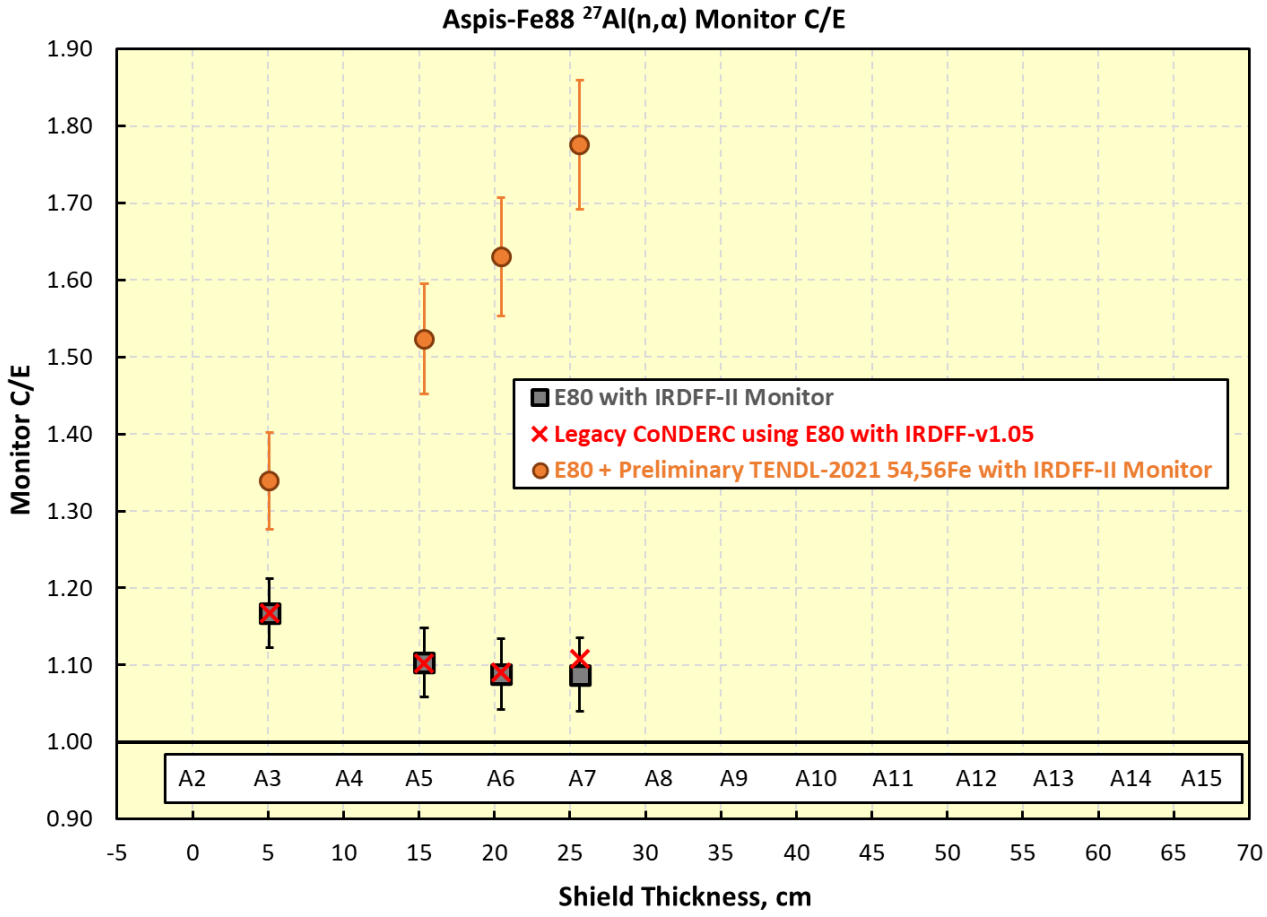

In conclusion, when using the preliminary TENDL-2021 ^{54,56}Fe nuclear data (i) the ^{32}S(n,p) C/E values are improved (although a constant bias remains); (ii) the ^{103}Rh(n,n') and ^{115}In(n,n') results are little changed; (iii) the Cd-covered ^{197}Au(n,γ) C/E values are shifted up several per cent, making some previously good results now high while improving the lower C/E values observed for deep penetration; and (iv) the previously poor ^{27}Al(n,α) results are significantly worse.